Effect of Mn^{2+} concentration in ZnS nanoparticles on photoluminescence and electron-spin-resonance spectra

P. H. Borse
Centre for Advanced Studies in Material Science and Solid State Physics, Department of Physics, University of Pune, Pune 411 007, India

D. Srinivas, R. F. Shinde, and S. K. Date
Physical Chemistry Division, National Chemical Laboratory, Pune 411 008, India

W. Vogel
Fritz-Haber-Institut der Max-Planck-Gesellschaft, Faradayweg 4-6, D-14195 Berlin, Germany

S. K. Kulkarni
Centre for Advanced Studies in Material Science and Solid State Physics, Department of Physics, University of Pune, Pune 411 007, India

(Received 13 August 1998; revised manuscript received 21 January 1999)

Organically capped zinc sulfide nanoparticles doped with different manganese concentrations were prepared under similar conditions. Only the doping concentration was varied. Photoluminescence and electron-spin-resonance (ESR) investigations show some new results. At an optimum concentration of Mn doping a maximum in the photoluminescence is reached, whereas photoluminescence quenching occurs at higher concentrations. ESR investigations show that the spectra arise due to four different contributions of Mn ions, viz., (1) Mn(S_I) in tetrahedral cationic substitution site with T_d symmetry, (2) isolated Mn ions at the surface or interstitial locations (S_{II}) with octahedral symmetry (O_h), (3) Mn-Mn dipolar interactions (S_{III}), and (4) exchange-coupled Mn clusters (S_{IV}) in various proportions. Linewidths for all these (S_I–S_{IV}) differ from each other. Identification of these components suggests that S_I may be responsible for the photoluminescence increase, whereas S_{II}–S_{IV} may be responsible for the luminescence quenching in nanoparticles.
[S0163-1829(99)02335-8]

Photoluminescence (PL) and electroluminescence (EL) properties of Mn-doped II-VI semiconductors, especially those of ZnS, have been widely investigated. A considerable amount of work has also been devoted, using electron-spin-resonance (ESR) technique, to obtain an insight about the local crystal-field effects and symmetry around the Mn ions. It is thus well known[1–3] that Mn^{2+} ions occupy Zn^{2+} lattice sites in the ZnS host lattice. In the PL process an electron from the ZnS valence band is excited across the band gap. The photoexcited electron subsequently decays by a nonradiative recombination process to some surface or defect site, or it is captured by Mn^{2+} ions in the $^4T_1$ level from which it decays radiatively to the $^6A_1$ level. In fact doping with Mn reduces the probability of nonradiative recombination and causes the ZnS to phosphor at about 590 nm by a radiative recombination transition between $^4T_1$ and $^6A_1$. It was proposed in a model by Bhargava *et al.*[4] that in nanocrystalline Mn-doped ZnS the transition between $^4T_1$ and $^6A_1$ is enhanced due to quantum confinement effects. It was suggested that the coupling of $3d$ states of Mn ions and *sp* states of ZnS nanoparticles gives rise to a fast transfer of photoexcited electrons from the ZnS band to the localized Mn states and the Mn ion derived states, due to the increased overlap of wave functions in nanoparticles. They showed that the radiative transition is about 5 orders of magnitude faster in nanoparticles compared to that in the bulk. Surface passivation of nanoparticles also helps to enhance the photoluminescence due to the reduction of available nonradiative recombination centers. Oka and Yanata[5] also have studied Mn-doped superlattices of CdTe and microcrystals of CdS. They interpret their results in terms of quantum confinement and agree that nanostructures enhance the luminescence efficiency. This has been recently challenged by Bol and Meijerink.[6] They conclude from the lifetime measurements and time-resolved spectroscopy that the nanoparticles do not form a new class of luminescent materials as decay time is not altered from the corresponding bulk material. More experiments may be required to assess the efficiency of nanoparticles as luminescent materials in future. In this paper we restrict to the issue of effect of Mn ion concentration on photoluminescence and ESR spectra.

Although Mn ions in nanocrystallites go to substitutional sites, in a similar way as the Mn ions in the bulk ZnS lattice, changes in the bond length occur,[7] which are size dependent. In order to probe the local effects around the Mn site, Kennedy *et al.*[8] studied the ESR of two nanocrystal samples of ZnS doped with Mn. They observed in one case (NC1) a broad peak on which six characteristic peaks of the Mn ion held in a cubic host lattice were superimposed. Spectral broadening was attributed to Mn-Mn interaction or aggregates of nanocrystals or more than one Mn ions in a crystallite. In the other sample (NC2), a six line spectrum characteristic of isolated Mn^{2+} in cubic lattice was recorded. From their[8] spectra (values of g and hyperfine splitting constants

TABLE I. g factor, fine-structure parameter D, and hyperfine splitting parameter $|A|$ for Mn^{2+} in ZnS lattice. X denotes no fine splitting.

Sample	g factor	D (cm^{-1})	$\|A\|$ (10^{-4} cm^{-1})
ZnS (cubic) (Ref. 2)	2.0025	0	64
ZnS (hex.) (Ref. 2)	2.0016	0.0105	65
ZnS NC1 (Ref. 8)	2.003	X	64.5
ZnS NC2 (Ref. 8)	2.001	0.05-0.10	89
ZnS signal I (Ref. 10)	2.0024	not determined	64.5
ZnS signal II (Ref. 10)	2.0013	not determined	84.0
Sample A, B (this work)	$2.001(\pm 0.00005)$	0.0001	63.9
Sample C, D (this work)	$2.001(\pm 0.00005)$	X	$90.0(\pm 0.5)$
Sample E (this work)	2.0025	X	$90.0(\pm 0.5)$

are given in Table I) and by comparison with those of Mn^{2+} ions in a glassy matrix by Griscom and Griscom,[9] they conclude that such ESR spectra are characteristic of nanocrystalline materials in a glassy host. For the second sample (NC2) they conclude that Mn^{2+} ions are isolated and are on the surface of the nanoparticles. There is, however, not much discussion about the accurate determination of the structure in the two samples they investigated. Igarashi, Isobe, and Senna [10] agreed with the findings in Ref. 8. In a recent paper Levy *et al.*[11] also attribute the changes in their ESR spectra to the changes in Mn sites but differ from Bhargava *et al.*[4] in the interpretation about the enhanced photoluminescence in their $Cd_{0.95}Mn_{0.05}S$ nanocrystals. We observed increase and decrease in photoluminescence depending upon the Mn doping concentration in ZnS nanoparticles. We have synthesized ZnS nanoparticles under similar conditions and only Mn concentration is varied. This has resulted in the particles of similar size up to some Mn concentration that has enabled us to discuss the effects arising only due to the concentration changes of Mn. It was also possible to fit the ESR spectra with four types of Mn centers.

Synthesis of Mn-doped ZnS nanoparticles was carried out by the method described in detail in Ref. 12. Briefly, it is a chemical method in which aqueous solutions of $ZnCl_2$ and Na_2S are reacted with each other in the presence of an organic capping agent. Here mercaptoethanol is used as the capping agent. For doping the particles, $MnCl_2$ is added in various volume proportions to obtain the particles of different doping concentrations. Reactions were carried out in a nitrogen atmosphere. The precipitate thus obtained was washed several times with deionized water and air dried to obtain a free standing nanoparticle powder. The actual concentration of doped Mn was determined using a Baird Atomic Alfa-4 (U.K.) atomic absorption spectrometer. Although a large number of samples in the doping range of 0.008 Mn wt % to 7.598 Mn wt % were synthesized and investigated, only some typical samples [A (0.008 Mn wt %), B (0.0296 Mn wt %), C (0.7295 Mn wt %), D (2.003 Mn wt %), and E (7.598 Mn wt %)] are discussed here. Lower doping did not produce luminescent samples and higher doping resulted in multiphase samples and are not discussed further. UV absorption spectra were recorded using a Shimadzu UV 300 double beam spectrophotometer, which showed an excitonic peak at 290 nm, for the doped and undoped ZnS nanoparticle samples discussed here. Photoluminescence studies were carried out on a Perkin Elmer LS 50 model on these powder samples using an excitation wavelength of 290 nm. The results are qualitatively similar to what we have shown earlier[12] viz. at an optimum concentration of Mn there is a maximum in the photoluminescence intensity.

Structure analysis was carried out on a Huber powder x-ray diffractometer using CuK_{α_1} wavelength, and the patterns were analyzed by Debye function analysis (DFA). The calculated intensity of a set of randomly oriented model clusters of increasing size is added up using their number fractions as free parameters. Details of this method have been described elsewhere.[13] Figure 1(a) shows the diffraction pattern of sample A after correction for angular factors and rescaling to the reciprocal scattering vector **b**. Samples from A to C showed similar x-ray diffraction patterns. From the DFA analysis a nearly perfect fit was obtained for cubic ZnS-type clusters that contain one twin plane per cluster [solid curve in Fig. 1(a)]. Hexagonal wurtzite-type structures can be completely excluded. The cluster size falls in a narrow range of 2.5–3.2 nm as shown in the inset. The Zn-Zn interatomic distance was found to deviate by -1% from the bulk ZnS value of 0.3835 nm. Sample E shows [Fig. 1(b)] a complex mixture of larger particles with cubic as well as wurtzite structure along with some additional phases. Thus using Mn concentration up to ≈ 0.8 wt %, it is possible to obtain single cubic phase ZnS nanoparticles. However, beyond this, multiphase particles result. Particles also tend to be larger as is evident from sharp x-ray diffraction lines. Sample D is an intermediate state of C and E. These structural results will be published in more details elsewhere.

ESR spectra recorded for different Mn concentration are shown in Fig. 2(a). The spectra were recorded using a Burker EMX-X band spectrometer. The sample quantity was 60 mg in each case. The microwave frequency was 9.76 GHz, and a 100 kHz field modulation was used. At low Mn concentration of 0.008 Mn wt % (sample A), a characteristic six line pattern of Mn^{2+} in the cubic ZnS lattice appears. In a cubic ZnS lattice containing substitutional Mn^{2+}, hyperfine transitions are due to $\Delta \mathbf{M}_I = 0$, which give rise to characteristic six line spectrum. An additional fine structure should arise for the symmetry lower than the cubic due to transitions between $\Delta \mathbf{M}_s$: $\pm\frac{5}{2} \leftrightarrow \pm\frac{3}{2}$ and $\pm\frac{3}{2} \leftrightarrow \pm\frac{1}{2}$. The spin Hamiltonian can be written as

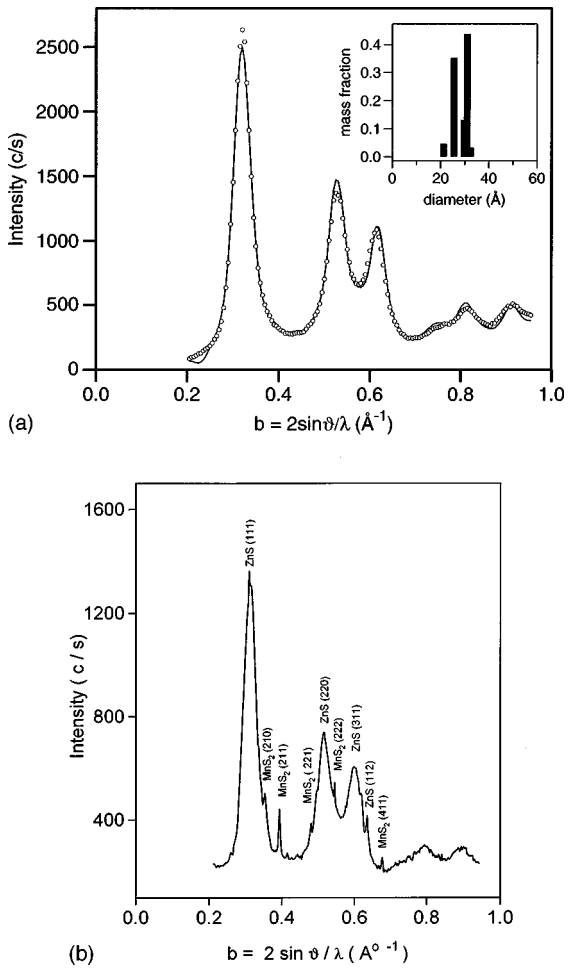

FIG. 1. (a) X-ray diffraction of mercaptoethanol capped ZnS nanoparticles (sample *A*) compared with the theoretical diffraction (solid line) of an assembly of single twined ZnS nanoparticles. The inset shows the mass fraction of individual clusters used for the simulation versus the size. (b) X-ray diffraction of mercaptoethanol capped ZnS:Mn nanoparticles (sample *E*).

$$H = g\beta \mathbf{H}\cdot\mathbf{S} + \tfrac{1}{6}a(S_x^4 + S_y^4 + S_z^4) + D[S_z^2 - \tfrac{1}{3}S(S+1)] + A\mathbf{S}\cdot\mathbf{I}. \quad (1)$$

Here β is the Bohr magneton, H is the applied magnetic field, and g, D, and $|A|$ are the ESR parameters. The first term in Eq. (1) is due to Zeeman interaction, the second due to cubic field, the third due to fine-structure splitting, and the fourth due to hyperfine interaction with the Mn nucleus. For Mn^{2+} with an electronic configuration of $t_{2g}^3 e_g^2$, the g tensor is isotropic and is close to the free spin g value (2.0023). For cubic crystal-field symmetry as in the case with zinc-blende structure, $D=0$, and for axial symmetry (wurtzite structure), D has a finite value.

Although at lower concentration of Mn doping (sample *A*), a six line spectrum as in Fig. 2(a) appears; a broad single peak (sample *E*) appears at higher concentration. Intermediate samples show complex spectra. Spectral simulation and deconvolution of all experimentally recorded ESR spectra was made using Bruker SIMFONIA AND WINEPR software package. The analysis has made us identify four types of Mn-related features in ESR spectra. The contribution of these features varies from sample to sample and depends upon the concentration of Mn ions being doped in the samples. At low Mn ion concentration (sample *A*) six line spectrum characteristic of cubic ZnS:Mn lattice arises due to substitutionally doped isolated Mn^{2+} ions in different nanoparticles. At very low Mn concentration, it is very likely that only some particles are doped perhaps with a single Mn ion, and spectral features arise due to $\mathbf{M}_s = |-\frac{1}{2}\rangle$ to $|+\frac{1}{2}\rangle$ transition coupled to Mn nuclear spin. In addition to allowed transitions $\Delta\mathbf{M}_s = \pm 1$ and $\Delta\mathbf{M}_I = 0$, forbidden transitions with $\Delta\mathbf{M}_I = \pm 1$ or ± 2 are also observed. The ESR spectra for all samples in the low Mn concentration range viz. 0.008–0.0201 Mn wt % could be fitted with two components viz. $\mathbf{S_I}$ and $\mathbf{S}_{II}$ for Mn^{2+} locations. However, both $\mathbf{S}_I$ or $\mathbf{S}_{II}$ have same g value (2.001). The $\mathbf{S}_I$ is characterized by smaller hyperfine interaction constant $|A_{\mathrm{Mn}}| = 63\times10^{-4}$ cm^{-1}, while the latter by larger $|A_{\mathrm{Mn}}| = 89\times10^{-4}$ cm^{-1}. $\mathbf{S}_I$ could be attributed to Mn^{2+} substituted in a Zn site while $\mathbf{S}_{II}$ to the surface/interstitial site. Value of linewidth (ΔH) for $\mathbf{S}_I$ is 9 G and $\mathbf{S}_{II}$ is 47 G. Double integration of the first derivative ESR spectra revealed that the intensity of $\mathbf{S}_I$ and $\mathbf{S}_{II}$ increases up to the 0.0345 Mn wt %. Thereafter the signal due to $\mathbf{S}_I$ disappears, and a dipolar broadened signal with a peak-to-peak linewidth of $\Delta H = 350$ G due to the interacting Mn centers ($\mathbf{S}_{III}$) appears. Figure 2(b) shows the deconvoluted and simulated ESR spectra for sample *B*. It is to be mentioned that the simulation software employed has certain limitations. It does not include $\mathbf{M}_I$ dependent linewidth anisotropy and the forbidden transitions. With further increase of Mn doping concentration [Fig. 2(a), sample *C*] a broad spectrum with six superimposed lines appears. Similar broad signals were also observed by Kennedy *et al.* The intensity of $\mathbf{S}_{III}$ increases, and there appears another isotropic signal with a peak-to-peak linewidth of $\Delta H = 204$ G ($\mathbf{S}_{IV}$). This signal corresponds to the exchange-coupled Mn^{2+} clusters. Figure 2(c) shows the deconvoluted and simulated spectra showing the presence of $\mathbf{S}_{II}$, $\mathbf{S}_{III}$, and $\mathbf{S}_{IV}$ sites in case of sample *D*. Sample *E* with 7.598 Mn wt % showed the spectrum with a major contribution arising from exchange narrowed $\mathbf{S}_{IV}$ centers. Levy *et al.*[11] observed an ESR peak similar to that of sample *E* for a $Cd_{0.95}$ $Mn_{0.05}$ S cluster. The shape in $Cd_{0.95}$ $Mn_{0.05}$ S clusters did not change even at 70 GHz. This may be due to the presence of $\mathbf{S}_{IV}$-type Mn interactions. Figure 3 shows how the contribution of different components $\mathbf{S}_I$ to $\mathbf{S}_{II}$ change with Mn concentration, and Fig. 4 illustrates how $\mathbf{S}_I$ to $\mathbf{S}_{IV}$ arise. It may be further added that for a very low concentration of Mn (up to 0.008 % Mn), where the contribution of $\mathbf{S}_{II}$ to $\mathbf{S}_{IV}$ is significantly low or zero, the PL intensity goes on increasing as more and more numbers of particles achieve a single Mn ion. Some particles may also receive Mn ions on their surfaces (but the ratio $\mathbf{S}_{II}/\mathbf{S}_I$ is low). This occurs up to the Mn concentration of about 0.0296 Mn wt %. With further increase in the Mn concentration, along with $\mathbf{S}_{II}$ to $\mathbf{S}_{IV}$ there will be some contribution of $\mathbf{S}_I$. However, due to dominance of $\mathbf{S}_{II}$, $\mathbf{S}_{III}$, and $\mathbf{S}_{IV}$ ($\mathbf{S}_{II}/\mathbf{S}_I \approx 6$), the contribution due to $\mathbf{S}_I$ will be negligible for Mn concentration higher than 0.0296% Mn.

Further analysis of the ESR spectra also leads to some interesting results. The g parameter and hyperfine interaction

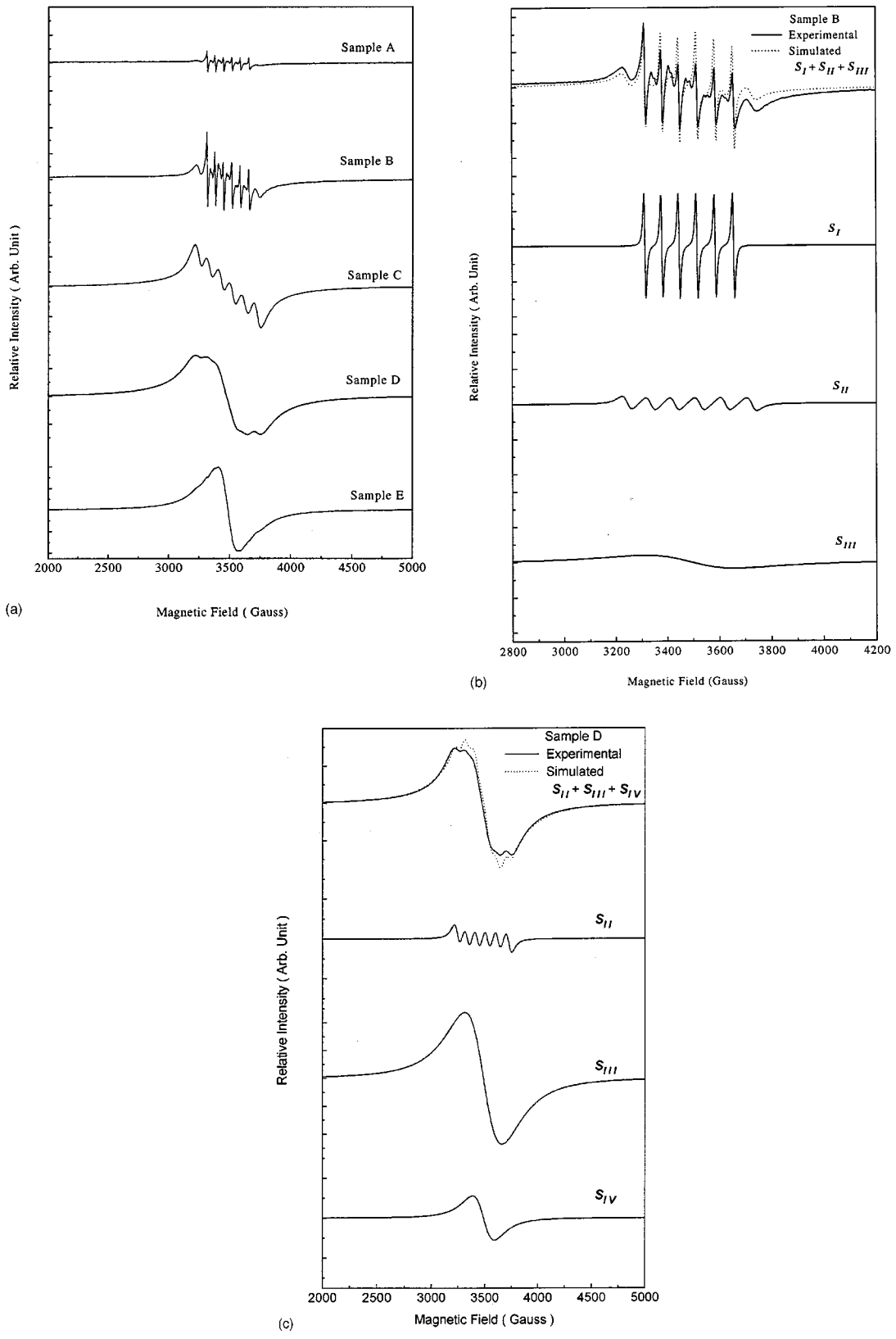

FIG. 2. Electron-spin-resonance spectra of Mn-doped ZnS nanoparticles recorded at 9.76 GHz frequency. (a) For samples *A* (0.008 Mn wt %), *B* (0.0296 Mn wt %), *C* (0.7295 Mn wt %), *D* (2.003 Mn wt %), and *E* (7.598 Mn wt %); (b) and (c) for sample *B* and sample *D* showing comparison of experimental and simulated curves along with the contribution from $\mathbf{S}_I$ to $\mathbf{S}_{IV}$ components.

constant $|A_{\mathrm{Mn}}|$ for samples *A* to *E* are listed in Table I along with the reported values for cubic and hexagonal ZnS doped with dilute amounts of Mn^{2+}. The *g* and $|A|$ values for cubic ZnS doped with Mn^{2+} are 2.0025 and 64×10^{-4} cm^{-1}, and those for hexagonal lattice are 2.0016 and 65×10^{-4} cm^{-1}, respectively. Some recent ESR experiments by Young, Poindexter, and Lyon[14] on differently prepared silicon nanocrystals, including porous silicon, have *g* values for nanocrystal-

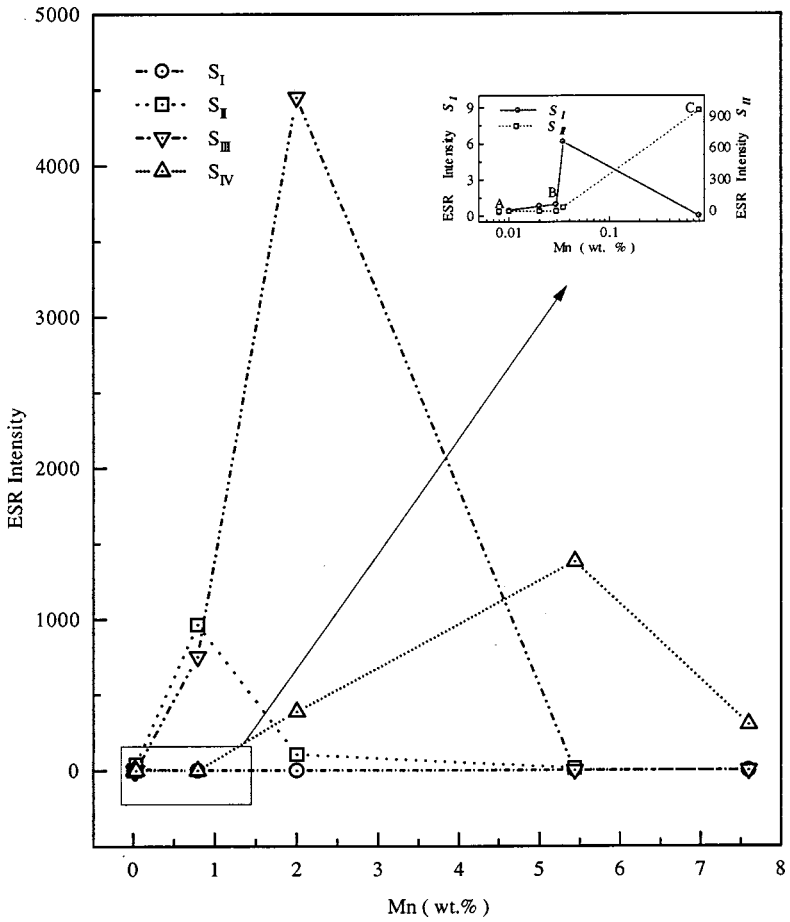

FIG. 3. Variation in ESR intensity of $\mathbf{S}_I$ to $\mathbf{S}_{IV}$ with concentration of Mn. The clipping shows how $\mathbf{S}_I$ and $\mathbf{S}_{II}$ ESR intensities vary for lower concentrations.

lites that are consistently lower than those of bulk silicon values. This has been attributed to quantum confinement of electrons in the nanoparticles. In view of these results, reduction in g value observed here can also be considered as a consequence of quantum confinement effect. The g value for samples A to D is 2.001 ± 0.00005. The hyperfine interaction constant for samples A to C is $63.9 \pm 0.5 \times 10^{-4}$ cm^{-1}, a value very close to that observed for bulk Mn-doped ZnS. This may be due to low concentration of Mn; only isolated Mn or $\mathbf{S}_I$-type component dominates here. For samples D and E we observe the dominance of $\mathbf{S}_{III}$ and $\mathbf{S}_{IV}$ components. Moreover, the ESR spectra result in a single peak after the concentration of 2.003 Mn wt %. The model proposed here depicts the observed trends.

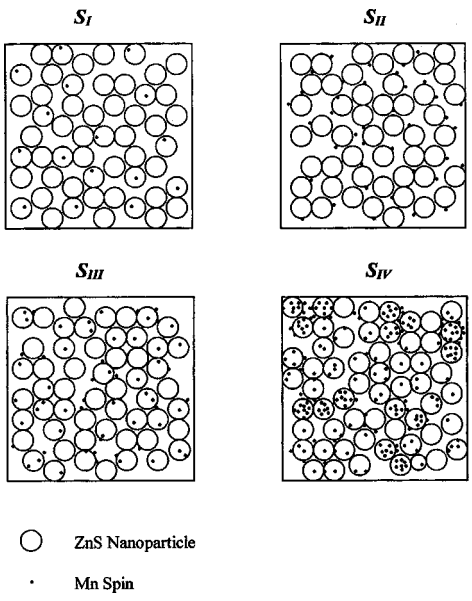

FIG. 4. Schematic diagram showing how the different centers from $\mathbf{S}_I$ to $\mathbf{S}_{IV}$ arise.

In summary, we have synthesized ZnS nanoparticles doped with Mn. An attempt is made to keep the size of ZnS particles constant (2.8 ± 0.4 nm) and change only the Mn concentration. The ESR spectra analysis leads to the understanding that there are four types of contributions, and their relative proportion varies with Mn concentration in the samples. At very low Mn concentration ($\mathbf{S}_I$), some particles are doped and some are not. With an increasing Mn concentration, more and more particles are doped increasing the photoluminescence intensity. This is similar to what has been observed by Hoffmann *et al.*[15] in CdS:Mn samples viz. at higher concentration Poisson statistics applies with zero doping for some particles, one Mn for some and two or more Mn for some particles. At low concentrations, of course, some particles are doped with one and others without any Mn. At higher concentration $\mathbf{S}_{II}$ to $\mathbf{S}_{IV}$ contributions increase accompanied by luminescence quenching. They are therefore likely to be major contributors in the luminescence quenching. The work presented in earlier papers was only on limited samples. Therefore, there was no scope for observing the kind of differences observed by us.

S.K.K. would like to thank UGC, India and ISRO, India for financial support. S.K.K. also thanks Professor A. M. Bradshaw for constant encouragement, and Fritz Haber Institut der Max-Planck-Gesellschaft, Berlin, Germany for financial support of her visit to Fritz Haber Institut. One of the authors (P.H.B.) also thanks ISRO for financial support. It is our pleasure to thank Professor V. G. Bhide and Dr. D. Cunningham for their valuable discussions and interest in this work.

[1] B. Bleaney and K. W. Stevens, Rep. Prog. Phys. **16**, 108 (1953).
[2] K. D. Bowers and J. Owen, Rep. Prog. Phys. **18**, 304 (1955).
[3] G. W. Ludwig and H. H. Woodbury, in *Solid State Physics*, edited by F. Seitz and D. Turnbull (Academic, New York, 1962), Vol. 13, p. 223.
[4] R. N. Bhargava, D. Gallagher, X. Hong, and A. Nurmikko, Phys. Rev. Lett. **72**, 416 (1994).
[5] Y. Oka and K. Yanata, J. Lumin. **70**, 35 (1996).
[6] A. A. Bol and A. Meijerink, Phys. Rev. B **58**, R15 997 (1998).
[7] Y. Wang, N. Herron, K. Moller, and T. Bein, Solid State Commun. **77**, 33 (1991); Y. L. Soo, Z. H. Ming, S. W. Huang, Y. H. Kao, R. N. Bhargava, and D. Gallagher, Phys. Rev. B **50**, 7602 (1994).
[8] T. Kennedy, E. R. Glaser, P. B. Klein, and R. N. Bhargava, Phys. Rev. B **52**, R14 356 (1995).
[9] D. L. Griscom and R. E. Griscom, J. Chem. Phys. **47**, 2711 (1967).
[10] T. Igarashi, T. Isobe, and M. Senna, Phys. Rev. B **56**, 6444 (1997).
[11] L. Levy, D. Ingert, N. Feltin, and M. P. Pileni, Adv. Mater. **10**, 53 (1998).
[12] M. Kundu, A. A. Khosravi, S. K. Kulkarni, and P. Singh, J. Mater. Sci. **32**, 245 (1997); A. A. Khosravi, M. Kundu, B. A. Kuruvilla, G. S. Shekhawat, R. P. Gupta, A. K. Sharma, P. D. Vyas, and S. K. Kulkarni, Appl. Phys. Lett. **67**, 2506 (1995).
[13] W. Vogel, J. Urban, M. Kundu, and S. K. Kulkarni, Langmuir **13**, 827 (1997).
[14] C. F. Young, E. H. Poindexter, and S. A. Lyon (unpublished).
[15] D. M. Hofmann, A. Hofstaetter, U. Leib, B. K. Meyer, and G. Counio, J. Cryst. Growth **184/185**, 383 (1998).